Structural and functional connectivity of the nondecussating dentato-rubro-thalamic tract

Kalen J. Petersen[1,2], **Jacqueline A. Reid**[3], **Srijata Chakravorti**[4], **Meher R. Juttukonda**[1], **Giulia Franco**[2], **Paula Trujillo**[2], **Adam J. Stark**[2], **Benoit M. Dawant**[4], **Manus J. Donahue**[1,2], and **Daniel O. Claassen**[1,2]

[1]Department of Radiology and Radiological Sciences, Vanderbilt University Medical Center, Nashville, TN, USA

[2]Department of Neurology, Vanderbilt University Medical Center, Nashville, TN, USA

[3]Meharry Medical College, Nashville, TN, USA

[4]Department of Electrical Engineering and Computer Science, Vanderbilt University, Nashville, TN, USA

Abstract

The dentato-rubro-thalamic tract (DRTT) regulates motor control, connecting the cerebellum to the thalamus. This tract is modulated by deep-brain stimulation in the surgical treatment of medically refractory tremor, especially in essential tremor, where high-frequency stimulation of the thalamus can improve symptoms. The DRTT is classically described as a decussating pathway, ascending to the contralateral thalamus. However, the existence of a nondecussating (i.e. ipsilateral) DRTT in humans was recently demonstrated, and these tracts are arranged in distinct regions of the superior cerebellar peduncle. We hypothesized that the ipsilateral DRTT is connected to specific thalamic nuclei and therefore may have unique functional relevance. The goals of this study were to confirm the presence of the decussating and nondecussating DRTT pathways, identify thalamic termination zones of each tract, and compare whether structural connectivity findings agree with functional connectivity. Diffusion-weighted imaging was used to perform probabilistic tractography of the decussating and nondecussating DRTT in young healthy subjects from the Human Connectome Project (n=91) scanned using multi-shell diffusion-weighted imaging (270 directions; TR/TE=5500/89 ms; spatial resolution=1.25 mm isotropic). To define thalamic anatomical landmarks, a segmentation procedure based on the Morel Atlas was employed, and DRTT targeting was quantified based on the proportion of streamlines arriving at each nucleus. In parallel, functional connectivity analysis was performed using resting-state functional MRI (TR/TE=720/33 ms; spatial resolution=2 mm isotropic). It was found that the decussating and nondecussating DRTTs have significantly different thalamic endpoints, with the former preferentially targeting relatively anterior and lateral thalamic nuclei, and the latter connected to more posterior and medial nuclei (p<0.001). Functional and structural connectivity

---

*Corresponding author: Daniel O. Claassen, Village at Vanderbilt, 1500 21st Ave. S., Suite 3000, Nashville, TN 37212, daniel.claassen@vanderbilt.edu, Tel: 615-936-1007, Fax: 615-343-3946.

Conflicts of interest: The authors declare no relevant conflicts of interest.

measures were found to be significantly correlated (r=0.45, p=0.031). These findings provide new insight into pathways through which unilateral cerebellum can exert bilateral influence on movement and raise questions about the functional implications of ipsilateral cerebellar efferents.

1. Introduction

The dentato-rubro-thalamic tract (DRTT) links cerebellar efferents with white matter tracts ascending from the thalamus to the motor cortex, premotor cortex (Middleton and Strick, 1998), and supplementary motor area (Wiesendanger and Wiesendanger, 1985), where they regulate fine movement. The DRTT is one of the major outflow pathways of the cerebellum. It originates in the dentate nucleus, a major gray matter deep cerebellar structure, passes through the superior cerebellar peduncle, decussates in the midbrain and synapses at the contralateral red nucleus. From the red nucleus, the DRTT ascends to the thalamus, and connects to the ventral intermediate nucleus, where it synapses with neurons ascending to the cortex.

The classically described DRTT is a decussating pathway (d-DRTT); however, recent work applying deterministic fiber tractography in healthy subjects and human brain microdissection has shown the existence of an ipsilateral or nondecussating DRTT (nd-DRTT) (Meola et al., 2016). The discovery of uncrossed fibers in humans is an important advance in cerebellar anatomy. While primate (Wiesendanger and Wiesendanger, 1985), rodent (Aumann and Horne, 1996), and feline (Flood and Jansen, 1966) anatomical studies have demonstrated the existence of some non-crossing fibers from the dentate nucleus to the ipsilateral cortex, the nd-DRTT in humans remains virtually unstudied.

To ascertain the function of this pathway, it is essential to better characterize its structure. Meola *et al.* noted that the d-DRTT and nd-DRTT occupied different portions of their shared white matter bundles, with the nd-DRTT following a more dorsal trajectory in the superior cerebellar peduncle (SCP). This finding suggests that spatial segregation of the pathways may extend beyond the peduncle and into the thalamus. The thalamus is a dense and anatomically complex structure containing numerous white and gray matter sub-regions. In such a heterogeneous area, it is critical to know precisely which thalamic loci serve which cerebellar motor circuits.

Dysfunction of the DRTT is implicated in the emergence of tremor, where thalamic-targeted deep-brain stimulation (DBS) can ameliorate tremor in patients. Clinical correlates of DRTT impairment include essential tremor, the most common adult movement disorder, Parkinson's disease (Alesch et al., 1995), and multiple sclerosis (Torres et al., 2010). For DBS surgery, diffusion tractography can preoperatively define the thalamic endpoint of the DRTT (Coenen et al., 2014, 2011; Fenoy and Schiess, 2017), and successful DRTT stimulation is associated with improved motor outcomes (Schlaier et al., 2015). However,

previous studies employing tractography measures have focused exclusively on the d-DRTT (e.g. Kwon *et al.*, 2011; Anthofer *et al.*, 2014), even though unilateral cerebellar activity exerts bilateral effects on movement and cortical activity (Amrani et al., 1996; Cho et al., 2012; Cui et al., 2000; Immisch et al., 2003; Küper et al., 2012).

The conservation of the nd-DRTT across mammalian taxa suggests an unknown functional role for this pathway, perhaps in the coordination of bilateral movements, or as a compensatory system for movement after unilateral cerebellar damage. To identify the nd-DRTT's functional role, its subcortical anatomy must first be defined in greater detail. Thus, we examined its thalamic connectivity in comparison to the d-DRTT. We utilized 1.25-mm-resolution multi-shell diffusion-weighted magnetic resonance imaging (MRI) data from the Human Connectome Project (HCP) to identify thalamic nuclei that are preferentially targeted by the d-DRTT and nd-DRTT. To test whether functional connectivity between the cerebellar dentate nuclei and their ipsilateral and contralateral thalamic targets reflects d-DRTT and nd-DRTT structure, we utilized baseline (resting-state) blood oxygenation level-dependent (BOLD) functional MRI (fMRI) to quantify functional connectivity both ipsilaterally and contralaterally in the same cohort of healthy subjects.

2. Methods

2.1. Subject recruitment

HCP data for healthy subjects were obtained from the WU-Minn consortium 500 subjects release (Van Essen et al., 2013) (n=91; age=29.3±3.3 years; sex=54 F, 38 M).

2.2. Imaging

HCP diffusion-weighted brain images were acquired at 3.0 Tesla in a Siemens Skyra scanner. HCP images were acquired using 2D echo-planar readout with 270 directions (TR/TE=5500/89 ms; spatial resolution=1.25 mm isotropic). A multishell diffusion scheme was used with b-values of 1000, 2000, and 3000 sec/mm^2 (Sotiropoulos et al., 2013; Uğurbil et al., 2013). Scan time was approximately 55 minutes. Resting-state BOLD fMRI scans were acquired (TR/TE=720/33 ms; 1200 volumes; spatial resolution=2 mm isotropic) (Smith et al., 2013) in the same volunteers.

2.3. Image processing

Diffusion and functional images were pre-processed by the Human Connectome Project according to the procedures described in (Glasser et al., 2013). As part of the pre-processing pipeline, diffusion data were corrected for motion, echo planar imaging distortion, and eddy currents. fMRI pre-processing included distortion correction, motion correction, intensity normalization, and registration of fMRI series to Montreal Neurological Institute (MNI) 2-mm standard space. Subsequent image processing and analysis were performed using the FMRIB software library (FSL) (FMRIB, Oxford, UK) and custom Matlab scripts. We brain-extracted the pre-processed diffusion images with the 'BET' utility with fractional intensity threshold set to 0.3 (Smith, 2002). T_1- and T_2-weighted images were also brain-extracted using 'BET.' Fractional anisotropy (FA) values were calculated from the diffusion images, b-values, and b-vectors using the 'dtifit' tool.

To reduce contribution from cardiac and respiratory signals in the fMRI data, as well as random high-frequency fluctuations, we also applied high-pass and low-pass temporal filtering to exclude frequencies outside the 0.01-0.15 Hz range. fMRI data were spatially smoothed using a Gaussian kernel with a full-width-half-maximum of 5 mm.

2.4. Region of interest definition

Tractographic seed and waypoint regions for all subjects were hand-drawn excepting the thalami, which were automatically segmented, and inspected by a board-certified neurologist (DOC). The dentate nucleus was drawn on FA images in the coronal view, identified as a hypointensity in local FA values, representing a grey matter region surrounded by white matter, approximately 15 mm from the midline, lateral and posterior to the fourth ventricle. The superior cerebellar peduncle waypoint masks were drawn in single coronal slices on the FA maps, while the red nucleus was defined in axial T_2-weighted images as the hypointense ellipsoid area in the medial brainstem. The gross thalamus was segmented in native T_1 space using FSL-'FIRST' (Patenaude et al., 2011). All regions were drawn or segmented bilaterally.

2.5. Thalamic nuclei segmentation

Intrathalamic segmentation was carried out with a novel statistical shape model method constructed using high-field (7.0T) MR images from 9 healthy volunteers (Liu et al., 2015). The inputs to the subthalamic shape model are the whole thalamus, previously segmented by 'FIRST,' and a known correspondence between the native T_1 space and the shape model space, which was generated by a combination of rigid (Maes et al., 1997) and nonrigid (Rohde et al., 2003) registration. The final segmentation results are 23 distinct intrathalamic nuclei on each hemisphere in the native T_1 image space. An example of thalamic segmentation is shown in Fig. 1. A 3D version of the same segmentation can be found in NIfTI format in Fig. S1. Further comment on the validity and accuracy of this method can be found in the Discussion.

2.6. Image registration

T_1-weighted images were linearly registered to diffusion space using FSL's 'flirt' tool with 12 degrees of freedom (Jenkinson et al., 2002). The inverses of the resultant affine matrices were used to transform thalamus and red nucleus masks to diffusion space. T_1-weighted images were also non-linearly registered to the 2-mm MNI-152 brain using FSL's 'fnirt' tool, and warp parameters preserved.

2.7. DRTT tractography

The DRTT was defined by probabilistic fiber tractography with FSL's diffusion toolbox 'Fdt' (Behrens et al., 2007, 2003), which allows multiple fibers per voxel, permitting robust detection of crossing fibers. Probabilistic tractography was utilized in lieu of deterministic tractography since the goal was to build a quantitative distribution of fiber endpoints in the thalamus rather than to find a single small zone of maximum connectivity. First, diffusion parameters at each voxel were modeled using 'bedpostx,' which builds up a distribution of diffusion directions at each voxel using Bayesian estimation. Then, fiber-tracking was

performed with 'probtrackx2.' Four tracts were defined per subject: left d-DRTT (i.e. originating in left dentate and terminating in right thalamus), right d-DRTT, left nd-DRTT, right nd-DRTT. The dentate nuclei served as the seed regions, with the SCP, red nucleus, and thalamus as sequential forced-order waypoints. Step length was set at 0.5 mm with a maximum of 320 steps per fiber (this value was empirically determined as sufficient for both d-DRTT and nd-DRTT to reach the thalamus). No curvature threshold was set, since the presence of three waypoint masks was sufficient to exclude any streamlines deviating from the main track. 5000 streamlines were calculated per tract, per subject. Track maps were then registered to subject T_1 space, and then to MNI space, using the affine transformation matrix and then the warp coefficients generated from structural image registration.

2.8. Thalamic centers-of-gravity

For each MNI-space track-map, a thalamic center-of-gravity measure was calculated to estimate the locus of maximum connectivity for each tract. Center-of-gravity measures for d-DRTT and nd-DRTT were obtained by weighting all intra-thalamic voxels by the number of streamlines passing through each, and computing a weighted mean, thus producing a single Cartesian point, per subject, representing the 'center' of d-DRTT or nd-DRTT structural connectivity. These computations were performed on MNI-space-transformed tracks for spatial comparability.

2.9. Structural connectivity analysis

Mapping structural connectivity to thalamic nuclei was performed in subject T_1-weighted space. Because more streamlines completed tracking for the nd-DRTT than the d-DRTT, likely due to hindrance by crossing fibers in the d-DRTT, statistical analysis was performed on the percentage of the total streamlines arriving at each thalamic nucleus rather than the absolute number of streamlines. Because thalamic nuclei differed in size, percentage structural connectivity was adjusted proportionally to size of the target nucleus. A custom Matlab script was used to calculate the adjusted percentage for each thalamic nucleus; this measure defined structural connectivity. Left and right structural connectivity values were averaged, as laterality was not of interest. Nuclei accounting for 5% or more of the total structural connectivity with the d-DRTT, nd-DRTT, or both were considered to have high structural connectivity. This threshold was chosen because the median structural connectivity accounted for by a given nucleus was 1.9% and 1.2% for d-DRTT and nd-DRTT, respectively (see Results), and hence nuclei with 5% or higher had structural connectivity several times greater than the typical value. Finally, for each thalamic nucleus, we calculated the ratio of d-DRTT structural connectivity to nd-DRTT structural connectivity, a quotient we term structural d/nd ratio. A ratio above 1 indicates that a greater proportion of decussating fibers contact a given nucleus, while a ratio below 1 indicates the opposite. For instance, a nucleus in which a typical voxel received 12% of d-DRTT streamlines and 6% of nd-DRTT streamlines would have a structural d/nd ratio of 2.0.

2.10. Functional connectivity analysis

All functional connectivity analysis was performed in standard space. Timecourses were extracted from the left and right dentate nuclei, which were defined in MNI space using a probabilistic atlas available in FSL (Diedrichsen et al., 2011). These timecourses were then

used as inputs in subject-level connectivity modeling using FSL-fMRI Expert Analysis Tool ('FEAT'), in which the activity at each brain voxel is fit to the dentate nucleus timecourse. Voxelwise group-level functional connectivity was assessed with a 1-sample t-test using FSL's randomise function. Thalamic voxels with mean functional connectivity values (i.e. temporal correlations with the dentate timeseries) greater than 0.3 or less than -0.3 were included in group-level analysis, and t-statistics reported. We employed this threshold to eliminate weak correlations, similar to the approach in (Long et al., 2016). To assign functional connectivity according to the thalamic shape atlas, z-statistics for each nucleus were calculated using the Fisher transform. Functional d/nd ratio was defined for each of the 23 nuclei by dividing the d-DRTT z-statistic by the nd-DRTT z-statistic.

2.11. Statistics and hypothesis testing

The major hypothesis was that the d-DRTT and nd-DRTT differ in thalamic connectivity. This hypothesis was tested by comparing thalamic centers of gravity between d-DRTT and nd-DRTT. Center-of-gravity x- and y-coordinates in MNI space for the d-DRTT and nd-DRTT were compared using two-tailed t-tests, and p-values reported. To compare structural connectivity for each of 23 thalamic nuclei, we used a two-tailed, paired Student's t-test to assess whether d-DRTT connectivity was significantly different from nd-DRTT connectivity. Resultant p-values were then corrected for multiple comparisons using false discovery rate (FDR)<0.05 (Benjamini and Hochberg, 1995). Only p-values significant after FDR correction are reported. Structural and functional d/nd values were compared across the 23 nuclei using a Spearman's correlation.

3. Results

3.1. Fiber tracking

Probabilistic tractography for the d-DRTT and nd-DRTT was successful in all subjects, in that at least some fibers completed tracking from the dentate to the thalamus. 54.5% more streamlines completed tracking from dentate to thalamus for the mean nd-DRTT than the mean d-DRTT. Fig. 2 depicts both pathways in axial slices, as well as in a three-dimensional streamline representation. Fig. 2B was generated using Diffusion Toolkit and TrackVis (Cui et al., 2000). Averaged d-DRTT and nd-DRTT maps (left and right) are also available in digital NIfTI neuroimaging format as Fig. S2.

3.2. Thalamic centers of gravity

The nd-DRTT structural centers-of-gravity were more posterior in the thalamus than the d-DRTT by an average of 1.8 mm in MNI space (p<0.001), and more medial by 2.42 mm (p<0.001). (Table 1). A list of center-of-gravity coordinate for all subjects is available as File S1.

3.3. Cerebello-thalamic structural connectivity

8 of 23 thalamic nuclei examined exhibited high structural connectivity with either d-DRTT, nd-DRTT, or both. These were: centromedian, parafascicular, ventral anterior, ventral lateral anterior, ventral medial, ventral posterior lateral, ventral posterior medial, and ventral posterior inferior. Of these 8 nuclei, all exhibited statistically significant biases in d/nd ratio,

either toward the d-DRTT (4/8; ventral anterior, ventral lateral anterior, ventromedial, and ventral posterior inferior), or nd-DRTT (4/8; centromedian, parafascicular, ventral posterior lateral, and ventral posterior medial) (p<0.001 for all) (Fig. 3).

3.4. Cerebello-thalamic functional connectivity

Whole-brain, un-thresholded group mean connectivity maps for the left and right dentate nucleus are available in 3D NIfTI format as Fig. S3 and S4, respectively. Within the thalamus, significant functional connectivity with the dentate nucleus occurred in a distinctive band which traversed the medial aspect of the bilateral thalami, regardless of ipsilateral or contralateral dentate seeding (Fig. 4). While the functional connectivity did not display the same clear anterior/posterior bifurcation between d-DRTT and nd-DRTT targeting as did structural connectivity, there was a statistically significant correlation between structural d/nd ratio and functional d/nd ratio across the 23 nuclei (Spearman's ρ=0.45, p=0.031) (Fig. 5), which indicates that for cerebello-thalamic connectivity, structural and functional measures independently confirm d-DRTT and nd-DRTT patterns of thalamic targeting. One nucleus (ventral posterior inferior) was an outlier for functional d/nd ratio according to Grubbs' test, and was omitted from Fig. 5; however, its inclusion or exclusion did not affect the statistical significance of the relationship. A full list of all structural and functional d/nd values used in this analysis is available as File S2.

4. Discussion

We have shown that the decussating and nondecussating DRTT pathways connect to distinct regions of the thalamus, and linked these to probable thalamic nuclei. The nd-DRTT sends a greater proportion of its fibers to regions which are more posterior and medial than the classical d-DRTT, suggesting that these two pathways may participate in discrete cerebello-cerebral circuits. This finding was reinforced by the identification of a strong positive relationship with functional connectivity measurements. These results are consistent with the idea of separable cerebellar "output channels" performing different functions in parallel (Middleton and Strick, 1998). Further tractography studies, with streamlines originating in the various thalamic nuclei, may help to test the hypothesis that the d-DRTT and nd-DRTT have different cortical termination zones. Conversely, the substantial overlap between the d-DRTT and nd-DRTT in medial thalamic zones argues that the two pathways also participate in some shared circuits, which may explain how unilateral signals in the thalamus can exert effects on bilateral limb movements (Ellerman et al., 1994; Jäncke et al., 1999; Soteropoulos and Baker, 2008), and how surgical intervention in unilateral thalamus can result in bilateral cerebellar ataxia (Chun and Chang, 2017).

These findings are likely to influence our understanding of the mechanisms of tremor reduction in stereotactic DBS. It is probable that a thalamic electrode placed unilaterally in the thalamus will activate some fibers of both the d-DRTT and nd-DRTT, thus exerting a more direct influence on bilateral cerebellar pathways that would be predicted from commissural interhemispheric connections alone. A straightforward way to test this principle would be to inactivate one-sided DBS electrodes in subjects with bilateral movement disorders, such as essential tremor, and monitor tremor severity in both the

ipsilateral and contralateral limb to determine if stimulation effects are bilateral when performing reaching and grabbing tasks. Future studies will also examine both white matter microstructural integrity and functional connectivity of the bilateral DRTT in patients with essential tremor and Parkinson's disease.

It is important to note that diffusion-based tractography alone is insufficient to fully establish or refute the existence of a white-matter pathway. The existence of the nd-DRTT was shown by a prior study which performed human brain microdissections in addition to diffusion imaging (Meola et al., 2016). We make no claim to have independently verified the existence of this pathway, but rather offer comment on its anatomy in light of prior existential claims. Our observations likely warrant a future examination of the thalamic termination of the pathway in post-mortem brains coupled with high-resolution diffusion imaging.

This finding should be considered in the context of several limitations. First, the thalamic segmentation applied here was an interpolative estimate based on a model created using high-field structural MRI. At typical field strength (3.0 Tesla or less), accurate and consistent intrathalamic segmentation on T_1 images is challenging due to insufficient contrast. Therefore, although our model is a reasonable approximation of thalamic nuclei, some inconsistencies with the actual structures are likely. Our method can identify 23 distinct nuclei according to the Morel convention (Morel et al., 1997). Cross-validation on a leave-one-out basis on 9 subjects confirmed that this hierarchical statistical shape model significantly improved upon simple single-atlas and multi-atlas segmentation methods and agreed most strongly with the manual delineations of the nuclei. Structural connectivity data on a separate cohort of 43 healthy subjects also validated the segmentation of the pulvinar nucleus (Chakravorti *et al.*, 2018), one of the largest nuclei groups of the thalamus. This approach has thus been shown to perform accurately and reliably on healthy volunteers, and therefore was chosen for our segmentation purposes.

The size of some thalamic nuclei presents another challenge. For smaller nuclei, such as the habenula, with a volume of around 30 mm^3, precise determination of connectivity from these images may be difficult, as has been noted with regards to fMRI studies (Lawson et al., 2013), since the structure is only a few voxels in size. Our findings are best interpreted in terms of broader spatial patterns of connectivity rather than narrowly at each thalamic nucleus. Nevertheless, the consistent results between structural and functional connectivity support the conclusion that even for relatively small connectivity targets, repeatable connectivity measures are obtainable, even with divergent imaging modalities.

In conclusion, we have demonstrated that the cerebellar efferent white matter pathway passing through the ipsilateral red nucleus makes a more posterior and medial contact in the thalamus than its contralaterally projecting equivalent, a finding which may have implications for the etiology and treatment of cerebellum-related tremors, and which raises interesting questions about the precise functional role of the nondecussating DRTT in movement coordination.

Supplementary Material

Refer to Web version on PubMed Central for supplementary material.

Acknowledgments

Abbreviations

BOLD	Blood oxygenation level-dependent
d-DRTT	Decussating dentato-rubro-thalamic tract (ipsilateral)
d/nd	Decussating/nondecussating connectivity ratio
DBS	Deep-brain stimulation
DRTT	Dentato-rubro-thalamic tract
FA	Fractional anisotropy
FDR	False discovery rate
FEAT	fMRI Expert Analysis Tool
fMRI	Functional magnetic resonance imaging
FSL	FMRIB Software Library
HCP	Human Connectome Project
MNI	Montreal Neurological Institute
MRI	Magnetic resonance imaging
nd-DRTT	Nondecussating dentato-rubro-thalamic tract (contralateral)
SCP	Superior cerebellar peduncle

## Citations

Alesch F, Pinter MM, Helscher RJ, Fertl L, Benabid AL, Koos WT. Stimulation of the ventral intermediate thalamic nucleus in tremor dominated Parkinson's disease and essential tremor. Acta Neurochir (Wien). 1995; 136:75–81. https://doi.org/10.1007/BF01411439. [PubMed: 8748831]

Amrani K, Dykes RW, Lamarre Y. Bilateral contributions to motor recovery in the monkey following lesions of the deep cerebellar nuclei. Brain Res. 1996; 740:275–284. https://doi.org/10.1016/S0006-8993(96)00899-2. [PubMed: 8973825]

Anthofer J, Steib K, Fellner C, Lange M, Brawanski A, Schlaier J. The variability of atlas-based targets in relation to surrounding major fibre tracts in thalamic deep brain stimulation. Acta

Neurochir (Wien). 2014; 156:1497–1504. https://doi.org/10.1007/s00701-014-2103-z. [PubMed: 24829155]

Aumann TD, Horne MK. Ramification and termination of single axons in the cerebellothalamic pathway of the rat. J Comp Neurol. 1996; 376:420–430. https://doi.org/10.1002/(SICI)1096-9861(19961216)376:3<420::AID-CNE5>3.0.CO;2-4. [PubMed: 8956108]

Behrens TEJ, Berg HJ, Jbabdi S, Rushworth MFS, Woolrich MW. Probabilistic diffusion tractography with multiple fibre orientations: What can we gain? Neuroimage. 2007; 34:144–155. https://doi.org/10.1016/j.neuroimage.2006.09.018. [PubMed: 17070705]

Behrens TEJ, Woolrich MW, Jenkinson M, Johansen-Berg H, Nunes RG, Clare S, Matthews PM, Brady JM, Smith SM. Characterization and Propagation of Uncertainty in Diffusion-Weighted MR Imaging. Magn Reson Med. 2003; 50:1077–1088. https://doi.org/10.1002/mrm.10609. [PubMed: 14587019]

Benjamini Y, Hochberg Y, Benjamini Y, Hochberg Y. Controlling the false discovery rate: a practical and powerful approach to multiple testing. J R Stat Soc B. 1995; 57:289–300. https://doi.org/10.2307/2346101.

Chakravorti S, Morgan VL, Trujillo P, Wirz-Gonzalez R, Dawant BM. A Structural Connectivity Approach to Validate a Model-based Technique for the Segmentation of the Pulvinar Complex. Submiss. 2017

Cho SS, Yoon EJ, Bang SA, Park HS, Kim YK, Strafella AP, Kim SE. Metabolic changes of cerebrum by repetitive transcranial magnetic stimulation over lateral cerebellum: A study with FDG PET. Cerebellum. 2012; 11:739–748. https://doi.org/10.1007/s12311-011-0333-7. [PubMed: 22161500]

Chun MH, Chang MC. Bilateral ataxia after tumor resection in a patient with a unilateral thalamic tumor. Neurol Asia. 2017; 22:85–88.

Coenen VA, Allert N, Mädler B. A role of diffusion tensor imaging fiber tracking in deep brain stimulation surgery: DBS of the dentato-rubro-thalamic tract (drt) for the treatment of therapy-refractory tremor. Acta Neurochir (Wien). 2011; 153:1579–1585. https://doi.org/10.1007/s00701-011-1036-z. [PubMed: 21553318]

Coenen VA, Allert N, Paus S, Kronenbürger M, Urbach H, Mädler B. Modulation of the Cerebello-Thalamo-Cortical network in thalamic deep brain stimulation for tremor: A diffusion tensor imaging study. Neurosurgery. 2014; 75:657–669. https://doi.org/10.1227/NEU.0000000000000540. [PubMed: 25161000]

Cui SZ, Li EZ, Zang YF, Weng XC, Ivry R, Wang JJ. Both sides of human cerebellum involved in preparation and execution of sequential movements. Neuroreport. 2000; 11:3849–53. https://doi.org/10.1097/00001756-200011270-00049. [PubMed: 11117502]

Diedrichsen J, Maderwald S, Küper M, Thürling M, Rabe K, Gizewski ER, Ladd ME, Timmann D. Imaging the deep cerebellar nuclei: A probabilistic atlas and normalization procedure. Neuroimage. 2011; 54:1786–1794. https://doi.org/10.1016/j.neuroimage.2010.10.035. [PubMed: 20965257]

Ellerman JM, Flament D, Kim SG, Fu QG, Merkle H, Ebner TJ, Ugurbil K. Spatial patterns of functional activation of the cerebellum investigated using high field (4 T) MRI. NMR Biomed. 1994; 7:63–68. https://doi.org/fmri_Mary M-Converted #89; Used to be #2195. [PubMed: 8068527]

Fenoy AJ, Schiess MC. Deep Brain Stimulation of the Dentato-Rubro-Thalamic Tract: Outcomes of Direct Targeting for Tremor. Neuromodulation Technol Neural Interface. 2017; 20:429–436. https://doi.org/10.1111/ner.12585.

Flood S, Jansen J. The efferent fibres of the cerebellar nuclei and their distribution on the cerebellar peduncles in the cat. Cells Tissues Organs. 1966; 63:137–166. https://doi.org/10.1159/000142786.

Glasser MF, Sotiropoulos SN, Wilson JA, Coalson TS, Fischl B, Andersson JL, Xu J, Jbabdi S, Webster M, Polimeni JR, Van Essen DC, Jenkinson M. The minimal preprocessing pipelines for the Human Connectome Project. Neuroimage. 2013; 80:105–124. https://doi.org/10.1016/j.neuroimage.2013.04.127. [PubMed: 23668970]

Immisch I, Quintern J, Straube A. Unilateral cerebellar lesions influence arm movements bilaterally. Neuroreport. 2003; 14:837–40. https://doi.org/10.1097/01.wnr.0000069060.85441.bb. [PubMed: 12858043]

Jäncke L, Specht K, Mirzazade S, Peters M. The Effect of Finger-Movement Speed of the Dominant and the Subdominant Hand on Cerebellar Activation: A Functional Magnetic Resonance Imaging Study. Neuroimage. 1999; 9:497–507. https://doi.org/10.1006/nimg.1998.0426. [PubMed: 10329289]

Jenkinson M, Bannister P, Brady M, Smith S. Improved optimization for the robust and accurate linear registration and motion correction of brain images. Neuroimage. 2002; 17:825–841. https://doi.org/10.1016/S1053-8119(02)91132-8. [PubMed: 12377157]

Küper M, Thürling M, Stefanescu R, Maderwald S, Roths J, Elles HG, Ladd ME, Diedrichsen J, Timmann D. Evidence for a motor somatotopy in the cerebellar dentate nucleus-An fMRI study in humans. Hum Brain Mapp. 2012; 33:2741–2749. https://doi.org/10.1002/hbm.21400. [PubMed: 21938757]

Kwon HG, Hong JH, Hong CP, Lee DH, Ahn SH, Jang SH. Dentatorubrothalamic tract in human brain: diffusion tensor tractography study. Neuroradiology. 2011; 53:787–791. https://doi.org/10.1007/s00234-011-0878-7. [PubMed: 21547376]

Lawson RP, Drevets WC, Roiser JP. Defining the habenula in human neuroimaging studies. Neuroimage. 2013; 64:722–7. https://doi.org/10.1016/j.neuroimage.2012.08.076. [PubMed: 22986224]

Liu Y, D'Haese PF, Newton AT, Dawant BM. Thalamic nuclei segmentation in clinical 3T T1-weighted Images using high-resolution 7T shape models. SPIE Med Imaging. 2015:94150E–94150E.

Long Z, Duan X, Mantini D, Chen H. Alteration of functional connectivity in autism spectrum disorder: effect of age and anatomical distance. Sci Rep. 2016; 6:26527. https://doi.org/10.1038/srep26527. [PubMed: 27194227]

Maes F, Collignon A, Vandermeulen D, Marchal G, Suetens P. Multimodality image registration by maximization of mutual information. IEEE Trans Med Imaging. 1997; 16:187–98. https://doi.org/10.1109/42.563664. [PubMed: 9101328]

Meola A, Comert A, Yeh FC, Sivakanthan S, Fernandez-Miranda JC. The nondecussating pathway of the dentatorubrothalamic tract in humans: human connectome-based tractographic study and microdissection validation. J Neurosurg. 2016; 124:1406–1412. https://doi.org/10.3171/2015.4.JNS142741. [PubMed: 26452117]

Middleton FA, Strick PL. Cerebellar output: motor and cognitive channels. Trends Cogn Sci. 1998; 2:348–354. https://doi.org/10.1016/S1364-6613(98)01220-0. [PubMed: 21227231]

Morel A, Magnin M, Jeanmonod D. Multiarchitectonic and stereotactic atlas f the human thalamus. J Comp Neurol. 1997; 387:588–630. https://doi.org/10.1002/(SICI)1096-9861(19971103)387:4<588::AID-CNE8>3.0.CO;2-Z. [PubMed: 9373015]

Patenaude B, Smith SM, Kennedy DN, Jenkinson M. A Bayesian model of shape and appearance for subcortical brain segmentation. Neuroimage. 2011; 56:907–922. https://doi.org/10.1016/j.neuroimage.2011.02.046. [PubMed: 21352927]

Rohde GK, Aldroubi A, Dawant BM. The adaptive bases algorithm for intensity-based nonrigid image registration. IEEE Trans Med Imaging. 2003; 22:1470–1479. https://doi.org/10.1109/TMI.2003.819299. [PubMed: 14606680]

Schlaier J, Anthofer J, Steib K, Fellner C, Rothenfusser E, Brawanski A, Lange M. Deep Brain Stimulation for Essential Tremor: Targeting the Dentato-Rubro-Thalamic Tract? Neuromodulation Technol Neural Interface. 2015; 18:105–112. https://doi.org/10.1111/ner.12238.

Smith SM. Fast robust automated brain extraction. Hum Brain Mapp. 2002; 17:143–155. https://doi.org/10.1002/hbm.10062. [PubMed: 12391568]

Smith SM, Beckmann CF, Andersson J, Auerbach EJ, Bijsterbosch J, Douaud G, Duff E, Feinberg DA, Griffanti L, Harms MP, Kelly M, Laumann T, Miller KL, Moeller S, Petersen S, Power J, Salimi-Khorshidi G, Snyder AZ, Vu AT, Woolrich MW, Xu J, Yacoub E, U urbil K, Van Essen DC, Glasser MF. Resting-state fMRI in the Human Connectome Project for the WU-Minn HCP Consortium. Neuroimage. 2013; 80:144–168. https://doi.org/10.1016/j.neuroimage.2013.05.039. [PubMed: 23702415]

Soteropoulos DS, Baker SN. Bilateral representation in the deep cerebellar nuclei. J Physiol. 2008; 586:1117–1136. https://doi.org/10.1113/jphysiol.2007.144220. [PubMed: 18187463]

Sotiropoulos SN, Jbabdi S, Xu J, Andersson JL, Moeller S, Auerbach EJ, Glasser MF, Hernandez M, Sapiro G, Jenkinson M, Feinberg DA, Yacoub E, Lenglet C, Van Essen DC, Ugurbil K, Behrens TEJ. Advances in diffusion MRI acquisition and processing in the Human Connectome Project. Neuroimage. 2013; 80:125–143. https://doi.org/10.1016/J.NEUROIMAGE.2013.05.057. [PubMed: 23702418]

Torres CV, Moro E, Lopez-Rios AL, Hodaie M, Chen R, Laxton AW, Hutchison WD, Dostrovsky JO, Lozano AM. Deep Brain Stimulation of the Ventral Intermediate Nucleus of the Thalamus for Tremor in Patients With Multiple Sclerosis. Neurosurgery. 2010; 67:646–651. https://doi.org/10.1227/01.NEU.0000375506.18902.3E. [PubMed: 20647964]

Uğurbil K, Xu J, Auerbach EJ, Moeller S, Vu AT, Duarte-Carvajalino JM, Lenglet C, Wu X, Schmitter S, Van de Moortele PF, Strupp J, Sapiro G, De Martino F, Wang D, Harel N, Garwood M, Chen L, Feinberg DA, Smith SM, Miller KL, Sotiropoulos SN, Jbabdi S, Andersson JLR, Behrens TEJ, Glasser MF, Van Essen DC, Yacoub E. Pushing spatial and temporal resolution for functional and diffusion MRI in the Human Connectome Project. Neuroimage. 2013; 80:80–104. https://doi.org/10.1016/j.neuroimage.2013.05.012. [PubMed: 23702417]

Van Essen DC, Smith SM, Barch DM, Behrens TEJ, Yacoub E, Ugurbil K. The WU-Minn Human Connectome Project: An overview. Neuroimage. 2013; 80:62–79. https://doi.org/10.1016/j.neuroimage.2013.05.041. [PubMed: 23684880]

Wiesendanger R, Wiesendanger M. Cerebello-cortical linkage in the monkey as revealed by transcellular labeling with the lectin wheat germ agglutinin conjugated to the marker horseradish peroxidase. Exp Brain Res. 1985; 59:105–117. [PubMed: 4018190]
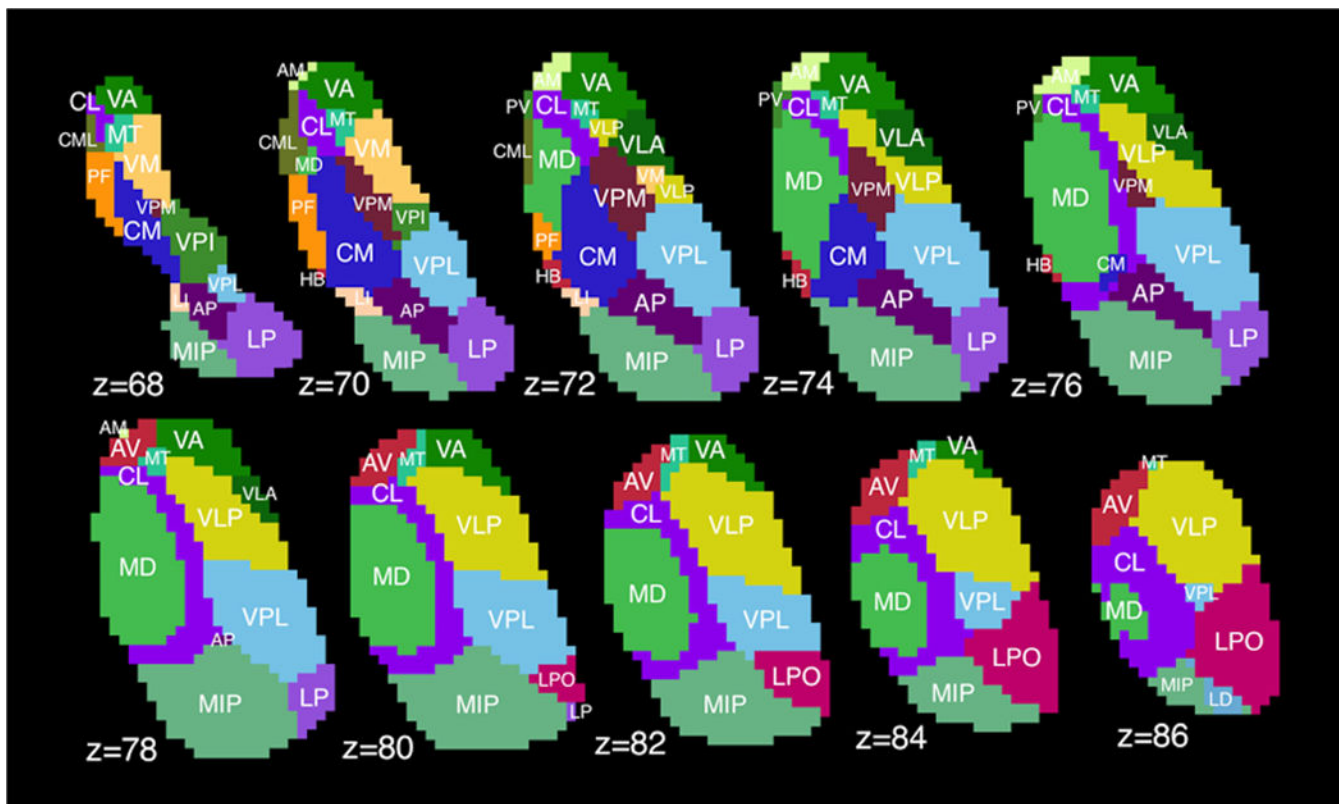
Fig. 1. Thalamic segmentation

Example of thalamic sub-segmentation using shape-fitting model based on Morel atlas. Displayed in MNI-1mm space; z represents slice number, not millimeters. VA=ventral anterior, CL=central lateral, MT=mammillothalmic tract, PF=parafascicular nucleus, CM=centromedian, VPM=ventral posterior medial, VPI=ventral posterior inferior, LI=limitans, AP=anterior pulvinar, VPL=ventral posterior lateral, MIP=medial+inferior pulvinar, LP=lateral pulvinar, AM=anteromedial, CML=central medial, HB=habenular, MD=mediodorsal, VLP=ventral lateral posterior, VLA=ventral lateral anterior, AV=anteroventral, LPO=lateral posterior, LD=lateral dorsal, PV=paraventricular, VM=ventral medial.
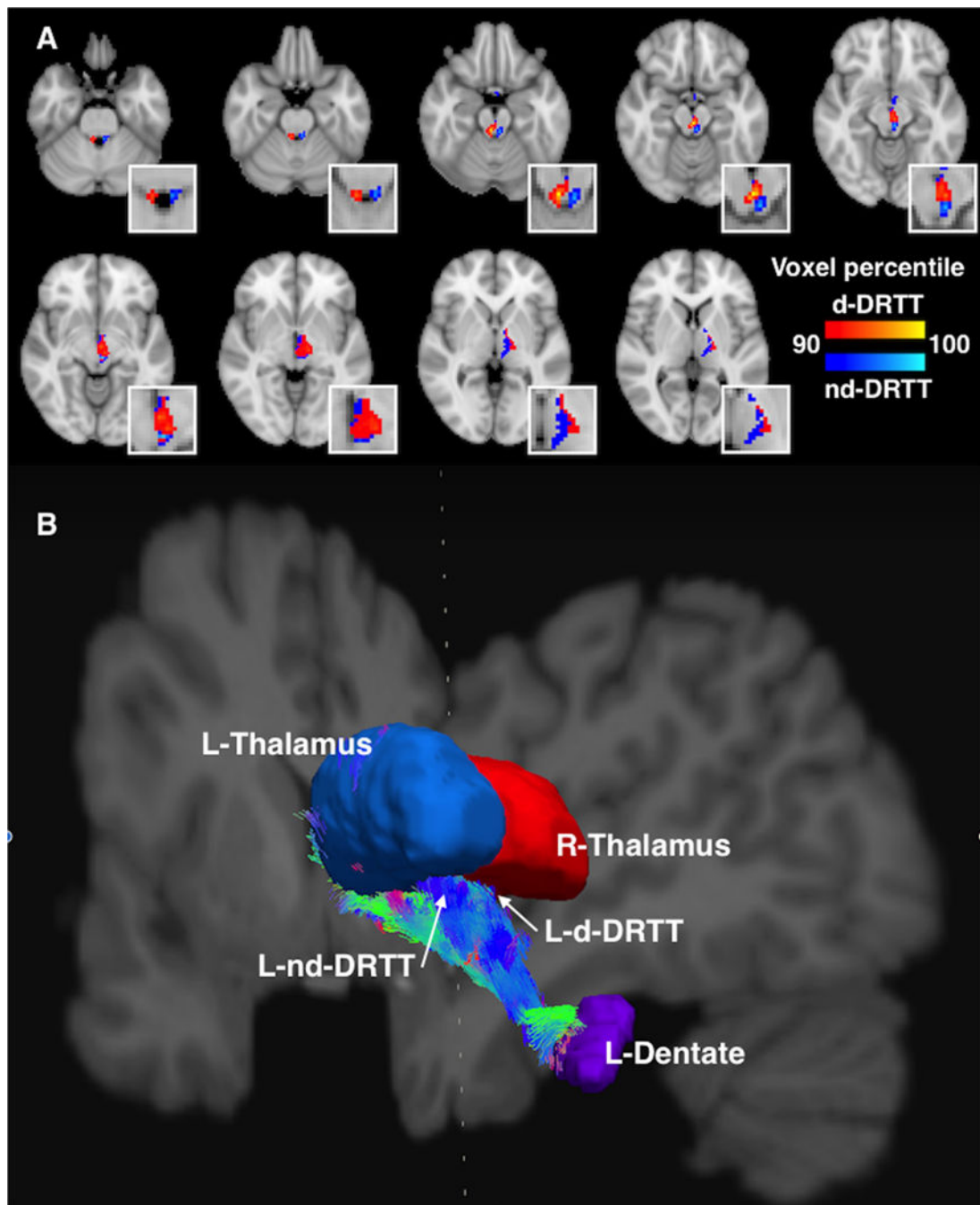
Fig. 2. The decussating and nondecussating DRTTs

A. Axial slices showing the d-DRTT (red) and nd-DRTT (blue), thresholded to include the top 10% of nonzero voxels by structural connectivity for each tract. For clarity, only the DRTT tracks arriving at the left thalamus (i.e. right decussating and left nondecussating tracts) are depicted. Figure has been up-sampled to 0.5mm isotropic resolution for better visualization clarity. Insets are enlargements of the same axial slices. **B.** A 3-dimensional visualization of the DRTT pathways originating in the left dentate nucleus and arriving at the ipsilateral (blue) and contralateral (red) thalamus. View is from the posterior aspect, with
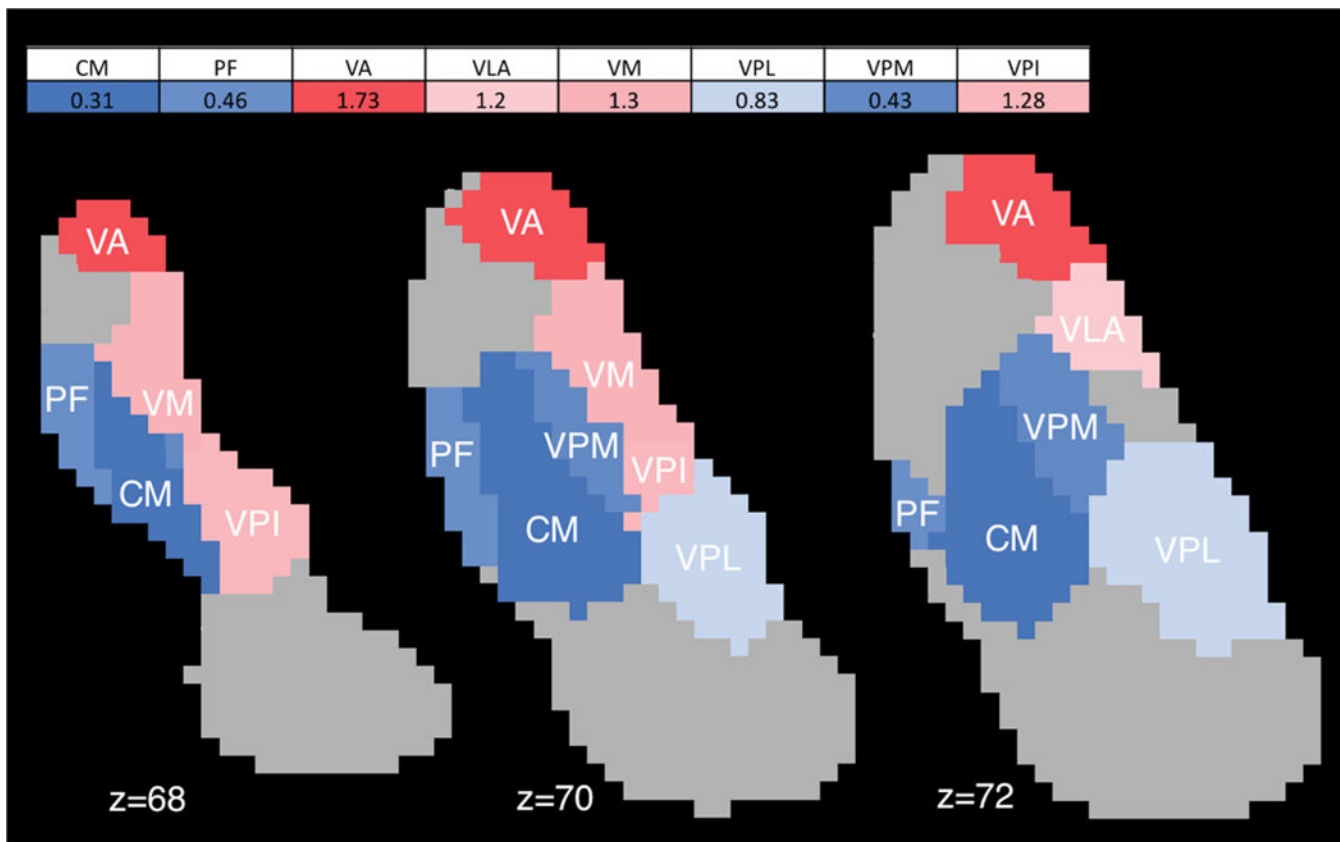
coronal and saggital slices of T_1-weighted image shown for reference. Streamline coloration is based on fiber orientation, where blue is superior-inferior, green is anterior-posterior, and red is left-right, per convention.
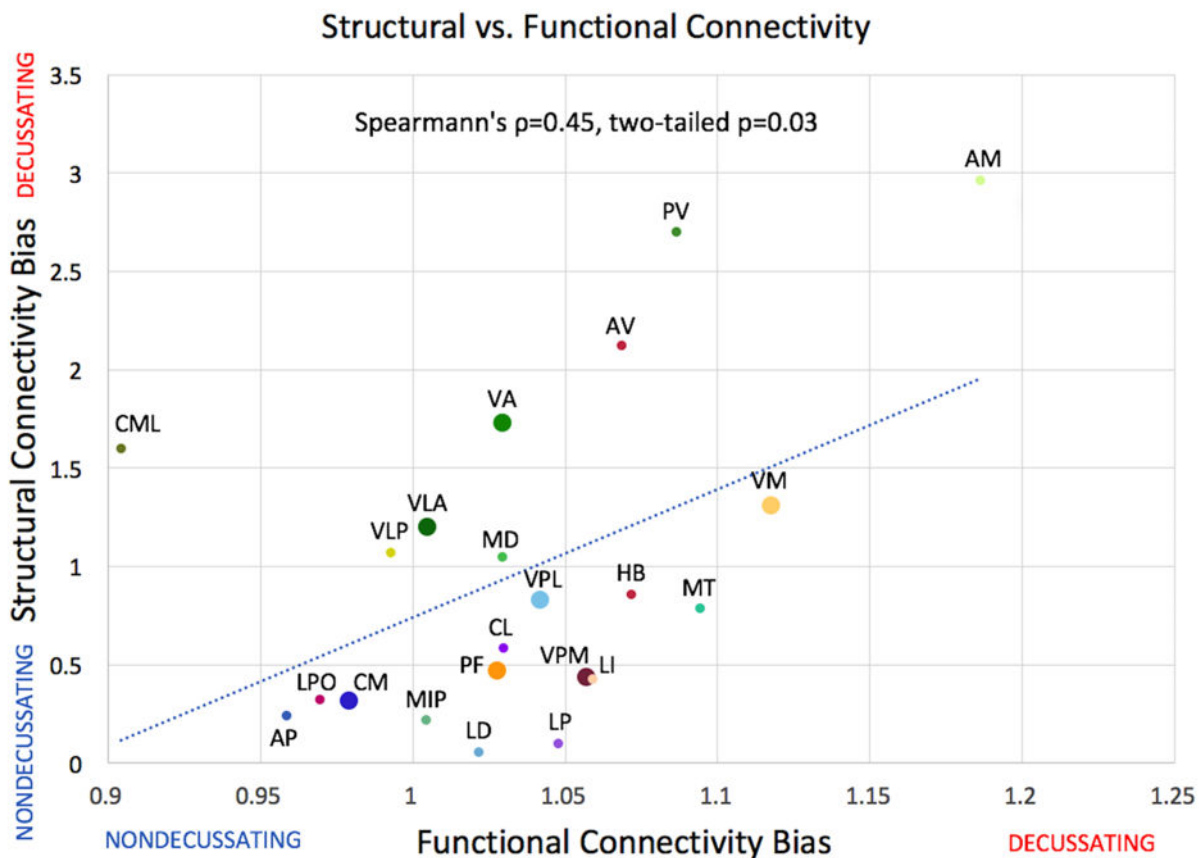
Fig. 3. DRTT thalamic structural connectivity

Map of structural d/nd ratios for thalamic nuclei with high (>5%) structural connectivity, and significant bias towards d-DRTT or nd-DRTT, in 1-mm MNI space. Blue indicates bias toward nd-DRTT, red indicates bias toward d-DRTT. Color intensity corresponds to degree of bias. Abbreviations: CM=centromedian; PF=parafascicular; VA=ventral anterior; VLA=ventral lateral anterior; VM=ventral medial; VPL=ventral posterior lateral; VPM=ventral posterior medial; VPI=ventral posterior inferior.
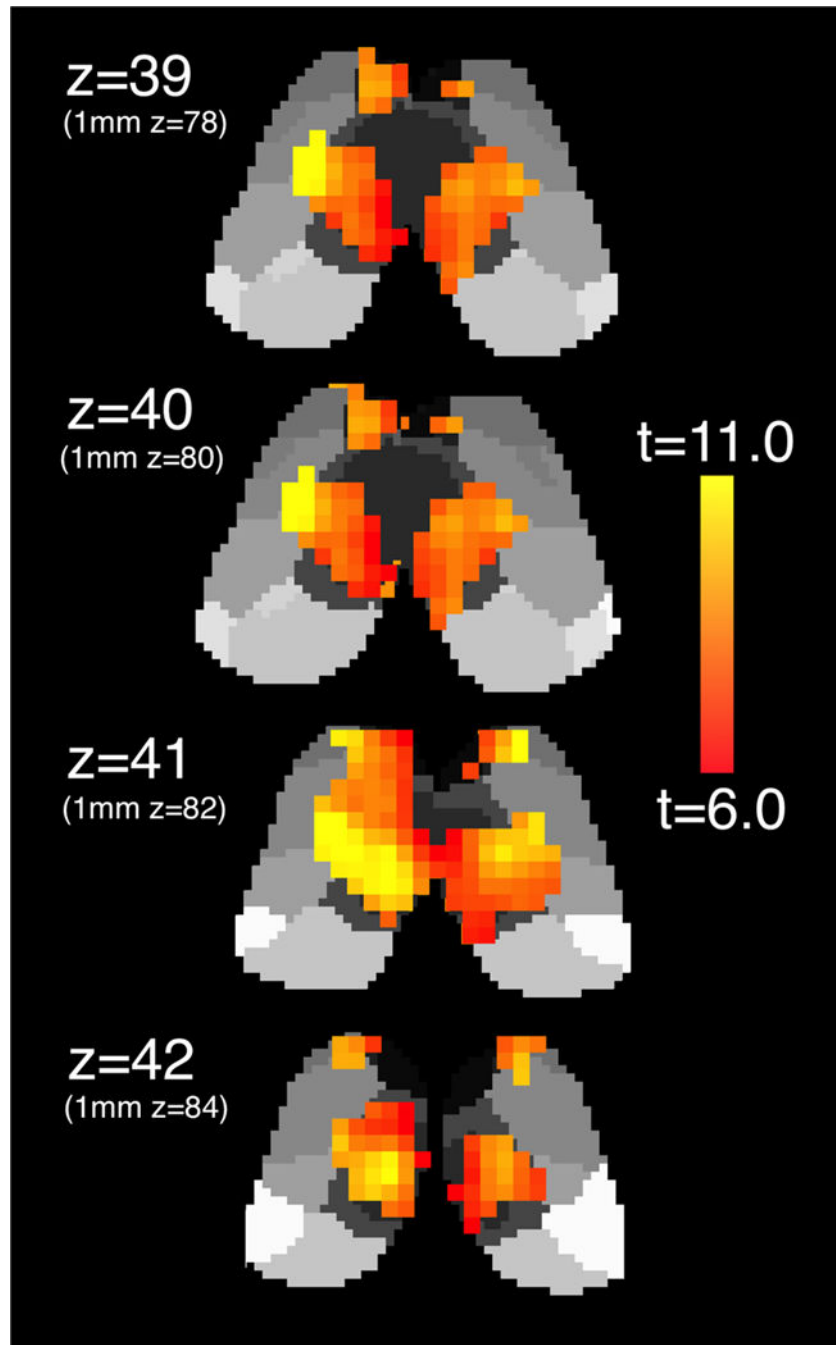
Fig. 4. Dentato-thalamic functional connectivity

Voxelwise functional connectivity of the unilateral dentate nucleus with bilateral thalamus in 2-mm MNI space. Left dentate connectivity displayed. 1-mm MNI equivalent z-slices listed in parentheses for comparison with Figs. 1 and 2.

Fig. 5. Relationship between structural and functional connectivity decussating / nondecussating bias across nuclei

Structural connectivity d/nd ratio shown on x-axis for 23 thalamic nuclei, functional d/nd shown on y-axis (unitless). Colors and labels correspond to Fig. 1. Enlarged points represent nuclei receiving 5% or more of streamlines after adjustment for size. One nucleus (VPI) was a statistical outlier according to Grubb's test and has been omitted from this figure; however, its inclusion or exclusion did not affect the statistical significance of the relationship.

Table 1

Thalamic mean centers of gravity (in MNI 2-mm space) for DRTT tracks.

	Center-of-gravity of structural connectivity values in thalamus		
	X	Y	Z
d-DRTT (l)	37.6	56.4	35.1
d-DRTT (r)	51.9	55.8	35.1
nd-DRTT (l)	50.9	55.0	35.2
nd-DRTT (r)	38.9	55.4	35.1
d-DRTT mean	n/a	56.1	35.1
nd-DRTT mean	n/a	55.2	35.2
d- minus nd- *	1.2 voxels	0.9 voxels	0.1 voxels
mm difference	2.4 mm	1.8 mm	0.2 mm
p-value	<0.001	<0.001	n.s.

*
Note: because x coordinates reflect left or right thalamus position, rather than location within the thalamus, x-coordinates were compared by distance from the midline (medial-lateral), rather than by absolute x-coordinate.